NANO LETTERS

2008
Vol. 8, No. 9
2998-3003

Quantitative Optical Trapping of Single Gold Nanorods

Christine Selhuber-Unkel

The Niels Bohr Institute, University of Copenhagen, Blegdamsvej 17, 2100 Copenhagen, Denmark

Inga Zins, Olaf Schubert, and Carsten Sönnichsen

Institute for Physical Chemistry, University of Mainz, 55099 Mainz, Germany

Lene B. Oddershede*

The Niels Bohr Institute, University of Copenhagen, Blegdamsvej 17, 2100 Copenhagen, Denmark

Received July 11, 2008; Revised Manuscript Received July 24, 2008

ABSTRACT

We report a quantitative analysis of the forces acting on optically trapped single gold nanorods. Individual nanorods with diameters between 8 and 44 nm and aspect ratios between 1.7 and 5.6 were stably trapped in three dimensions using a laser wavelength exceeding their plasmon resonance wavelengths. The interaction between the electromagnetic field of an optical trap and a single gold nanorod correlated with particle polarizability, which is a function of both particle volume and aspect ratio.

Gold nanoparticles are promising tools for optical applications in materials science and the life sciences due to their unusual optical properties which are caused by localized surface plasmon resonances.[1,2] At the plasmon resonance wavelength, collective oscillations of the conduction electrons lead to enhanced light absorption and scattering, so that particles down to a few nanometers in size can be detected with dark-field[3] and luminescence microscopy.[4] Varying the size and shape of the particles tunes the plasmon resonances over a wide range of wavelengths.[5]

In principle, gold nanoparticles can serve as substitutes for fluorescent marker molecules and quantum dots in biological experiments, an application that has attracted substantial interest in recent years. Big advantages of gold nanoparticles are their polarized light emission (for nanorods),[6] an enhanced fluorescence signal compared to single molecules,[4] and that they neither blink nor bleach.[7] In particular, rod-shaped gold nanoparticles are highly interesting candidates for luminescence and scattering studies as they show a suppressed interband damping[3] and can serve as orientation sensors due to their strong light polarization.[6] Using two-photon luminescence microscopy, gold nanorods have already been employed for in vitro and in vivo experiments[8] and for labeling cancer cells.[9] A further advantage of their usage in biological experiments is that gold nanorods are easily taken up by mammalian cells[10] and methods for a controlled functionalization of their surface have been developed.[11]

With optical tweezers, colloidal particles can be trapped in the focus of a laser beam and the optical forces acting on the particles can be measured with subpiconewton precision.[12] Typical optical tweezers probes are microscopic dielectric particles, such as latex microspheres, whose three-dimensional motion is strongly confined in an optical trap. It is also possible to trap nanometer-sized metallic particles, which are of particular interest for biological single molecule experiments, where a small probe size is imperative. Due to their strong polarizability compared to dielectric particles, metallic nanoparticles are ideal probes for optical tweezers experiments.[13] Gold spheres down to 18 nm in diameter[14] and silver spheres down to 20 nm in diameter[15] have been successfully trapped in three dimensions. First experiments have shown that it is also possible to confine the motion of individual gold nanorods with optical tweezers.[16,17] However, quantitative information on how an individual gold nanorod interacts with the electromagnetic field in an optical trap and how the optical forces depend on the size and aspect ratio of the nanorod has not been reported previously.

In this Letter we present quantitative information on the interaction between individual gold nanorods and the elec-

* Corresponding author. E-mail: oddershede@nbi.dk. Phone: +45 35325287. Fax: +45 35325425.

10.1021/nl802053h CCC: $40.75
Published on Web 08/23/2008

Table 1. Overview of Gold Nanorod Samples Used for Optical Trapping

diameter (nm)	length (nm)	aspect ratio	λ (nm)	volume (nm^3)	sample
8.3 ± 1	41.2 ± 8.3	5.0	876	2080	A
8.4 ± 1	47.3 ± 8.3	5.6	963	2466	B
13.1 ± 2.2	22.7 ± 5	1.7	750	2471	C
12.1 ± 2.5	35.7 ± 8.7	3.0	782	3641	D
10.7 ± 1.6	51.9 ± 7.6	4.9	909	4346	E
12.8 ± 2.5	41.5 ± 5.5	3.2	732	4791	F
13.8 ± 1.6	55.0 ± 7.8	4.0	799	7538	G
13.3 ± 1.9	59.3 ± 11.2	4.5	899	7623	H
13.1 ± 1.8	63.8 ± 10.4	4.9	871	8011	I
21.5 ± 5.9	46.6 ± 6.2	2.2	643	14244	J
19.4 ± 2.5	56.9 ± 4.7	2.9	696	14908	K
24.4 ± 4.5	57.9 ± 7.3	2.4	648	23271	L
27.1 ± 4.3	59.9 ± 6.5	2.2	644	29340	M
30.1 ± 4.7	56.9 ± 5.0	1.9	608	33349	N
36.5 ± 5.4	64.2 ± 13.3	1.8	614	54445	O
37.3 ± 5.0	63.8 ± 7.4	1.7	602	56129	P
36.8 ± 7.9	69.4 ± 8.1	1.9	611	60768	Q
44.1 ± 6.5	85.1 ± 7.3	1.9	632	107533	R

tromagnetic field of an optical trap. In particular, we determine the stiffness of the optical trap holding the nanorod in the trap for all three dimensions. This trapping stiffness follows a significantly different scaling compared to that observed for spherical gold and silver nanoparticles.[14,15] In contrast to previous studies on the trapping of gold nanorods, we were able to monitor the position of a single gold nanorod in the trap by recording the forward-scattered light of the particle with a quadrant photodiode so that the three-dimensional position signal of a nanorod in the trap could be followed and analyzed. Previously, only individual gold nanorods with a long axis of 48 nm were individually optically trapped.[16,17] We significantly expanded this range and trapped rods with lengths between 41 and 85 nm and widths between 8 and 44 nm. The particles with a diameter of 8 nm are the thinnest gold particles ever reported in optical trapping experiments. We demonstrate that the gradient forces holding the gold nanorods in the optical trap correlate with particle polarizability, which is a function of both particle volume and aspect ratio. We calculated the polarizabilities of the rod-shaped particles by employing the discrete dipole approximation (DDA) and compared them to our experimental results for the trapping stiffness.

All gold nanorod samples were prepared using the seeded growth method.[18] Small gold seeds were produced by reducing 10 mL of 0.5 mM hydrochloric acid ($HAuCl_4$, Sigma) with 600 μL of ice-cold 0.1 M sodium borhydride ($NaBH_4$, Sigma-Aldrich), a strong reducing agent, in the presence of 0.1 M cetyltrimethylammonium bromide (CTAB, Sigma). A growth solution was prepared by mixing 5 mL of 1 mM $HAuCl_4$ and 5 mL of 0.2 M aqueous CTAB solution. A small amount of 0.04 M silver nitrate ($AgNO_3$, Sigma-Aldrich) was added (typically in the range of 5−20 μL), followed by 70 μL of 0.0788 M ascorbic acid (Sigma-Aldrich). Finally, a small amount of preformed seed solution (typically 12 μL) was used to induce the growth of gold nanorods. For all preparations, deionized water (18 MΩ) was used. To achieve different sizes of the gold nanorods, the ratios between $HAuCl_4$, $AgNO_3$, and seed solution were adjusted.

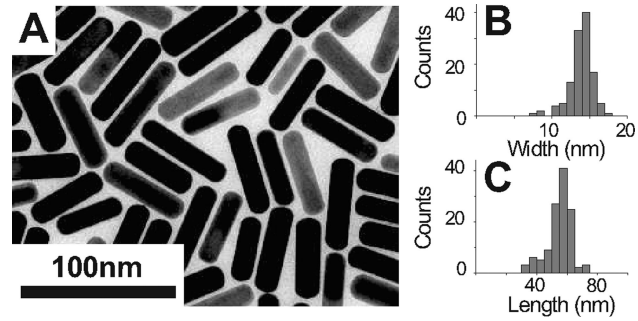

Figure 1. Transmission electron microscopy image of gold nanorods (A). Width (B) and length (C) distributions for the particles.

Using transmission electron microscopy (Philips CM-12 (120 kV) and Philips EM-420 (120 kV)), we determined the distributions of particle sizes in a particular sample. Histograms of length, width, and aspect ratio distribution were obtained by measuring the size of at least 100 particles per nanorod sample. A variety of samples was prepared, ranging from a length of 41.2 ± 8.3 nm (mean $\pm$ standard deviation) and a width of 8.3 ± 1 nm for the smallest particles to a length of 85.1 ± 7.3 nm and a width of 44.1 ± 6.5 nm for the largest particles. The aspect ratio of the particles was between 1.7 and 5.6. The average plasmon resonance wavelength was determined from optical ensemble extinction spectra and we found values between 602 and 963 nm. A summary of the properties of the particles used in this study is given in Table 1, and an example of a transmission electron micrograph of a particle sample is presented in Figure 1. Transmission electron micrographs and size distributions for the other samples are shown in Figure S1 (Supporting Information).

In order to prevent aggregation, we coated the particles with linear poly(ethylene glycol) (PEG) molecules by immersion in a 10 mM aqueous solution of *O*-[2-(3-mercaptopropionylamino)ethyl]-*O′*-methylpolyethylene glycol 5000 (Fluka 11124). To reduce the risk of trapping several particles simultaneously, the particles were further diluted in deionized water. A small fluid chamber (50 mm × 25 mm × 0.1 mm) consisting of two glass slides separated by Parafilm stripes and sealed with silicone grease served as sample chamber.

Single-beam optical tweezers were implemented with a Nd:YVO_4 laser (10 W Spectra Physics Millennia, $\lambda = 1064$ nm, TEM_{00}) in an inverted microscope (Leica DMIRB HC).[19] A quadrant photodiode (S5981, Hamamatsu) recorded the forward-scattered light of the trapped particles for approximately 3 s and the signal was further processed using custom-made Labview programs. Figure 2 shows a sketch of the optical tweezers setup. In all experiments we used an oil immersion objective from Leica (HCX PL Apo, 63×, NA = 1.32, ∞, 0.17) in combination with an immersion oil of refractive index $n = 1.54$ (Cargille, refractive index liquids set A). This immersion oil was chosen in order to minimize spherical aberrations and enhance trapping efficiency at the trapping plane 5 μm above the lower surface.[20] There, also the influence of the bottom glass surface due to hydrodynamic friction can be neglected for nanometer sized particles and consequently all our experiments were performed at this

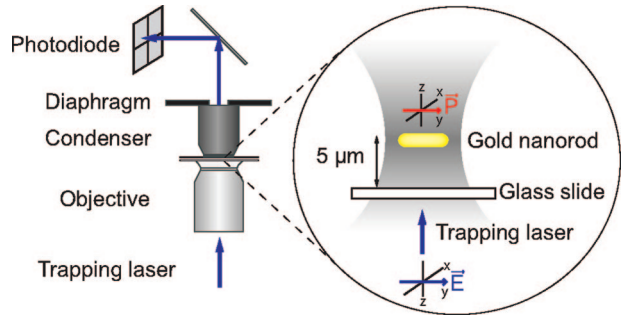

Figure 2. Illustration of the optical tweezers, the detection system, and the gold nanorod in the trap. $\vec{E}$ is the electric field vector of the laser, $\vec{P}$ is the direction of polarization.

trapping depth. For detection of the nanorod position along the direction of the propagating laser light, the opening of the condenser was optimized[21] and for the lateral measurements the condenser was fully open. For the data analysis, we assumed a linear relation between the photodiode signal and the position of the nanorod. This is valid, as long as the particle does not change alignment or tilt.[22] Depending on the size of the particle, laser powers between 60 and 230 mW (measured at the sample) were used for trapping. The exact choice of laser power was based on a consideration of using as little power as possible, yet having stable trapping of the particle for at least 10 min.

The total force on a single gold nanorod in an optical trap is composed of three different contributions: the gradient force, the absorption force, and the scattering force. The gradient force stabilizes and confines the position of the particle in the optical trap, whereas both the absorption and scattering force counteract a stable trapping and tend to push the particle out of the optical trap. Three-dimensional stable trapping is only possible if the gradient force exceeds the sum of absorption and scattering forces. The three forces depend on the electrical field squared, $\vec{E}^2$ (which is proportional to the intensity), the absorption cross section, C_{abs}, the scattering cross section, C_{scat}, and the Poynting vector, $\vec{S}$, and are given as:[23,24]

$$\vec{F}_{\mathrm{grad}} = \frac{1}{2}\alpha'(\omega)\nabla\langle\vec{E}^2\rangle \tag{1}$$

$$\vec{F}_{\mathrm{abs}} = \frac{n}{c}\langle\vec{S}\rangle C_{\mathrm{abs}} \tag{2}$$

$$\vec{F}_{\mathrm{scat}} = \frac{n}{c}\langle\vec{S}\rangle C_{\mathrm{scat}} \tag{3}$$

Here, $\alpha(\omega) = \alpha'(\omega) + i\alpha''(\omega)$ is the complex polarizability of the particle, n is the refractive index of the medium ($n = 1.33$), and c refers to the speed of light. C_{abs} and C_{scat} are related to the polarizability by

$$C_{\mathrm{scat}} = \frac{k_{\mathrm{w}}^4}{6\pi\varepsilon_0^2}|\alpha(\omega)|^2 \tag{4}$$

and

$$C_{\mathrm{abs}} = \frac{k_{\mathrm{w}}}{\varepsilon_0}\alpha''(\omega) \tag{5}$$

where $k_{\mathrm{w}} = 2\pi n/\lambda$ denotes the wave vector.[25]

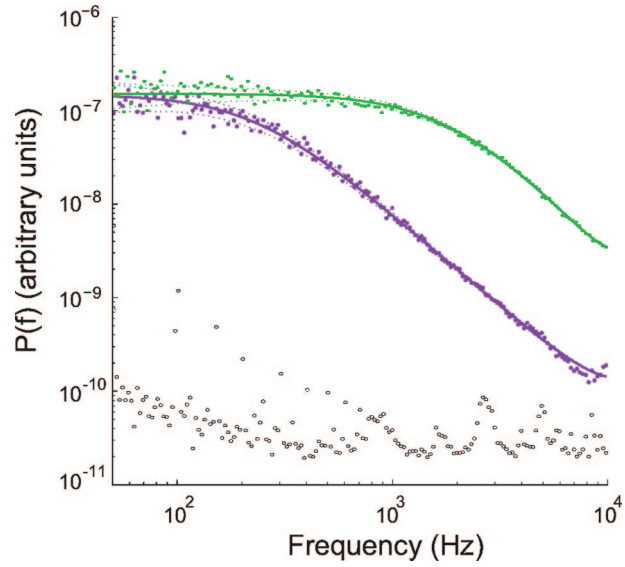

Figure 3. Power spectra for gold nanorods with length 85.1 ± 7.3 nm and width 44.1 ± 6.5 nm (green) and length 41.2 ± 8.3 nm and width 8.3 ± 1 nm (purple) at a laser power of 115 mW at the sample. The fits to the data are given by the full lines. Black circles show the power spectrum for an empty trap.

In each translational direction, x, y, or z, the intensity distribution in the laser focus is approximately Gaussian, so that the trapping potential is harmonic and the gradient force can be expressed by Hooke's law, for example, $F_x(x) = -\kappa_x(x - x_0)$ in the x direction. κ_x is the spring constant of the trapping potential in the x direction, x is the position of the particle, and x_0 is the equilibrium position of the particle. The Brownian motion of the particle is well-described by the Langevin equation, $m\ddot{x} = -\kappa_x x - \gamma\dot{x} + \mathcal{F}(t,T)$, where γ is the friction coefficient and $\mathcal{F}(t,T)$ is a time and temperature dependent white noise term stemming from random collisions of the object with surrounding molecules. By Fourier transformation of the Langevin equation, a Lorentzian power spectrum is obtained.

Due to their small size and rapid thermal motion, gold nanorods are not visible in a bright-field microscope. To determine whether or not a gold nanorod was optically trapped, we performed an online power spectral analysis of the photodiode signal. As is clear from Figure 3, the signal from an empty trap is significantly different from that of a rod in the trap. Figure 3 shows power spectra of the experimentally obtained time series of the largest and smallest trapped gold nanorod as well as that of an empty trap. Full lines are fits of Lorentzian functions to the data. In the fits we accounted for aliasing as well as for the filtering effect of the quadrant photodiode.[26−28] From the fitted value of the corner frequency, $f_c = \kappa/2\pi\gamma$, κ follows provided that γ is known.

To find γ in a particular direction for a particle of a certain size and nonspherical shape, it is necessary to know how the particle aligns with respect to that direction. In general, the orientation of asymmetric particles in an optical trap is a complicated issue. Depending on the size and shape of the particles, both an orientation along and perpendicular to the electric field is possible. Singer et al.[29] have shown that

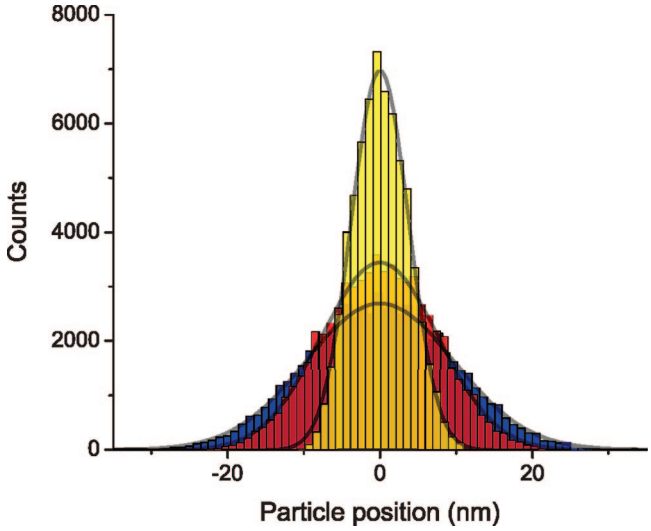

Figure 4. Three position histograms and their Gaussian fits showing subsequent parts of an experiment where particles (length, 85.1 ± 7.3 nm; width, 44.1 ± 6.5 nm) are diffusing into the trap. In the beginning of the experiments (yellow histogram) the standard deviation of positions is significantly smaller than in the middle (red histogram) and the end (blue histogram) of the experiment.

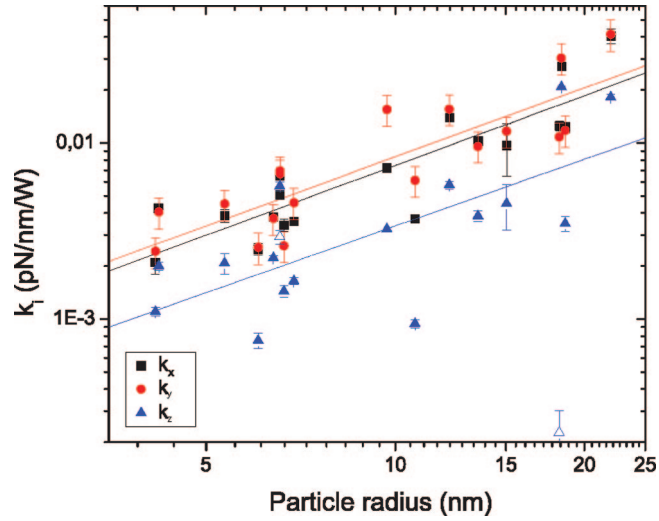

Figure 5. Results from the optical trapping experiments. Force constants of the particles in the optical trap were normalized to the laser power at the sample. The data are shown as a function of particle radius for the x direction (black), the y direction (red), and the z direction (blue). The slopes of the linear fits are 1.32 ± 0.18 for k_x, 1.30 ± 0.10 for k_y, and 1.26 ± 0.33 for k_z. Error bars correspond to standard deviations in the mean.

particles large compared to the beam waist tend to align along the direction of the propagating laser light, whereas smaller particles align along the $\vec{E}$-field orthogonal to the propagation direction of the laser light. In accordance with this are also the results reported by La Porta and Wang,[30] where quartz particles have been shown to rotate in a controlled fashion in an optical trap following the direction of a rotating $\vec{E}$-field. Recently, it has been shown that gold nanorods with a long axis of 48 nm also align with the electric field of the laser.[16] Because our particles are small compared to the diameter of the laser focus, which is about 1 μm, they are probably polarized along their long axis and oriented with the electric field of the trapping laser. Due to the plasmon resonances the long axis polarizability is much higher than the one for the short axis, so that an orientation along this axis is energetically more favorable. Thus, we assume the particles to be aligned with their long axis along the y axis, which is the direction of polarization in our setup. Figure 2 shows a sketch of the assumed orientation of a trapped nanorod.

The gold nanorods have the shape of a cylinder that is capped with two half-spheres (see Figure 1A), also called a spherocylinder. To calculate the values of the drag coefficient, γ, in the direction of the long axis and orthogonal to it, we used the drag coefficients for cylindrical particles, which is a good approximation for spherocylinders,[31,32] and neglected the PEG coating.

To load the optical trap with one gold nanorod, we waited until a particle diffused into the laser focus. It typically took 2−15 min before a particle entered the trap. The particles performed Brownian motion in the harmonic potential exerted by the optical trap. The distributions of particle positions are Gaussian, and their standard deviation increases stepwise with the number of particles in the trap.[14,15] Figure 4 shows position distributions from three different time intervals from the same experiment. The most narrow histogram stems from the initial part of the time series, when only a single rod was in the trap. As additional rods entered the trap, the histogram broadened. Hence, the standard deviation of a particular time series is a measure of how many particles are in the trap. All results reported in this Letter are from the observation of single rods in the trap.

While nanoscopic metallic particles are trapped, heating of the trapped object could become an issue.[33] Heating can decrease trapping stability or lead to bubble formation. Yet, heating of gold nanoparticles in optical traps has not been directly experimentally measured and reported. In our experiments, bubble formation or other signs of heating were never observed; hence the temperature in the water surrounding the gold nanoparticle is not as high as that predicted in ref.[33] This is probably due to two reasons: first, by compensating the spherical aberrations[20] we created an extremely efficient optical trap and used comparatively low laser powers. Second, the trapping wavelength was tuned to the long-wavelength side of the plasmon resonances of all particles, where the absorption cross section of the gold nanoparticles is significantly smaller than that at the resonance wavelength.[23] If trapping is done by a laser wavelength close to the resonance wavelength, the gradient force can no longer overcome the scattering and absorption forces.[16] However, particles can then be trapped by making use of their scattering with a Laguerre−Gaussian beam profile.[23]

Figure 5 shows experimental results for the trapping constants normalized by the laser power at the sample in x, y, and z directions as a function of smallest particle radius, r, in a double-logarithmic representation. z is the direction along the propagating laser light, y is the polarization direction, and x is orthogonal to both y and z (see definition of coordinate system in Figure 2). The spring constants in the x and y directions are similar, and the z direction is somewhat weaker. Overall, the absolute magnitude of the

spring constants is in the same range as those observed for trapping metallic spherical particles.[14,15] The plots reveal that the scaling relation between trapping constant and particle radius is significantly different from that known for spherical nanoparticles: for spherical metallic nanoparticles with radius smaller than the skin depth, the trapping constant is proportional to particle volume, and thus proportional to the polarizability according to the Clausius−Mossotti relation.[14,15] Thus, the slope of trapping constant versus particle radius in a double-logarithmic plot is 3 for small spherical metallic particles. Our results show a significantly slower increase with particle radius, namely, a slope of 1.3 even for the smallest observed gold nanorods in all three directions. The volume of a spherocylinder as a function of particle length, l, and radius, r, is given by $V(l,r) = (l - 2r)r^2\pi + 4/3r^3\pi$; hence, volume scales with the square of particle radius, r^2, for very long particles, and with r^3 for particles with small aspect ratio. Thus, trapping constant is not simply explained by only taking into account the particle volume. In other words, the strength of the interaction between the gold nanorod and the electromagnetic field in the optical trap, which is measured by trapping stiffness, does not scale directly with volume.

In Figure 6A the experimentally measured values for trapping constants in the x direction are shown as a function of particle volume. Clearly, the trapping constants increase with particle volume, but not by a simple linear relation, as observed for spherical gold and silver particles.[14,15] For comparison, the dashed line has a slope of 1 and represents the dependence on volume as it would be expected for spherical particles.

The observed interaction between a gold nanorod and the electromagnetic field can be understood in terms of particle polarizability, as the gradient force depends linearly on the real part of the particle polarizability, $\alpha'(\omega)$ (eq 1). For rod-shaped particles, the polarizabilities for both the long and the short axis are a function not only of particle volume but also of aspect ratio. We estimated $\alpha'(\omega)$ by calculating the absorption and scattering cross sections of the particle using the discrete dipole approximation (DDA), where a particle is approximated by a set of discrete dipoles. The resulting cross sections were resubstituted into eqs 4 and 5. DDA simulations were performed for plane wave excitation with a wavelength of 1064 nm with the freely available software ADDA[34,35] using spherocylinders as particle shape and water as surrounding medium. For the dielectric function, we used bulk values for gold given in Johnson and Christy.[36] We calculated the polarizability both for a rod aligned with the $\vec{E}$-field (denoted long axis in Figure 6) and with the propagation direction of the laser light (short axis).

The values of polarizability are plotted in Figure 6B as a function of particle volume. In the plot, we have also added the experimentally determined values for the trapping constant. The results from the simulation show that polarizability is strongly enhanced for the long axis and that plasmon resonances lead to a high dependence of the long-axis-polarizability on aspect ratio. Interestingly, similar deviations from a simple linear dependence are observed both

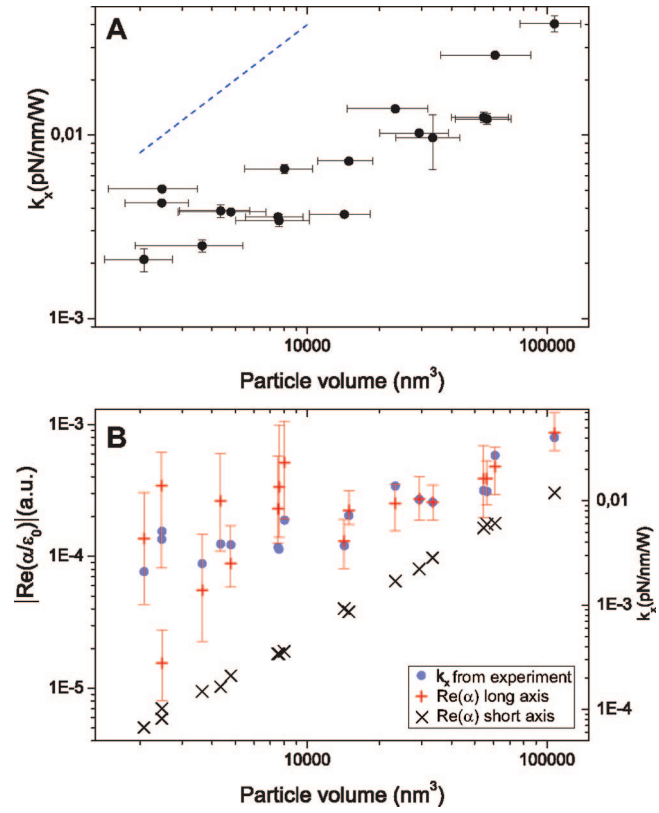

Figure 6. Comparison of experiment and theory. (A) Force constant k_x as a function of particle volume. Error bars correspond to standard deviations in the mean. The dashed blue line has slope 1 and is drawn for comparison. (B) Polarizability values are results from DDA calculations for alignment of the long axis of the rod with the $\vec{E}$-field (red crosses) and alignment of the short axis with the $\vec{E}$-field (black crosses). Error bars stem from the errors of the aspect ratios in the sample distributions. These are negligible for the short axis polarizability, as it is almost independent of aspect ratio. The experimental data for k_x are included in the graph (blue circles).

for the polarizability and for the experimental values of trapping stiffness. This is particularly evident for particle volumes larger than 10000 nm^3 and is consistent with an orientation of the particle's long axis with the $\vec{E}$-field. In contrast, if the short axis of the nanorod were aligned with the $\vec{E}$-field, an almost linear relation between particle volume and polarizability would be obtained, which is nearly independent of aspect ratio. We did not observe this in our experiments. For small particles, deviations from the sample average start to play a big role both in experiment and simulation, as indicated by the error bars for the calculated polarization parallel to the long axis. This can explain the discrepancies between simulation and experiment for small particles. Our results support previous results that a trapped nanorod is indeed aligned parallel to the $\vec{E}$-field.[16] Furthermore, the results show that the aspect ratio of the particles has significant impact on the polarizability and hence also on the trapping stiffness of the particles.

In an attempt to separate the volume dependence of the particle polarizability from its dependence on aspect ratio, we assumed that the particle polarizability can be cast as a product of a volume-dependent and an aspect ratio-dependent term

$$\alpha'\left(V, \frac{l}{2r}\right) = \alpha_1(V)\,\alpha_2\left(\frac{l}{2r}\right) \quad (6)$$

Because the polarizability of spheres is known to depend linearly on volume, and because the plasmon resonance wavelength for gold nanorods is mainly determined by aspect ratio and nearly independent of volume, it is reasonable to assume $\alpha_1(V) \sim V$. The DDA calculations support this assumption for the range of volumes and aspect ratios that is relevant in our experiments (see Figure S2, Supporting Information). The unknown function $\alpha_2(l/2r)$ can then be obtained from $\alpha_2(l/2r) = \alpha'(V,l/2r)/\alpha_1(V) \sim \alpha'(V,l/2r)/V$. Figure S3 (Supporting Information) shows the DDA calculations of α'/V as a function of aspect ratio. The experimentally obtained trapping constants k_x/V are also included. The DDA calculations of the polarizability suggest that $\alpha_2(l/2r)$ is an exponential function of aspect ratio. However, the experimentally obtained trapping constants do not correlate with aspect ratio, and in particular for large aspect ratios, deviations from the exponential fit are evident. This result indicates that the general relation between aspect ratio, volume, and polarizability is more complex than that expressed in eq 6.

In summary, we performed a quantitative analysis of the forces acting on individual optically trapped gold nanorods. Individual gold nanorods with diameters down to 8 nm and aspect ratios up to 5.6 were stably trapped for time spans exceeding tens of minutes by a laser which was tuned to the long-wavelength side of the plasmon resonances of the particles. The optical forces on the gold nanorods were seen to correlate with the polarizability and thus to depend both on volume and on aspect ratio of the rods in a nontrivial way. Our results show that gold nanorods can be used as efficient optical handles in nanoscale experiments. Hence, we anticipate our study to be a starting point for employing gold nanorods as force sensors in future quantitative in vitro and in vivo studies. Furthermore, with the force calibration routines presented here, biofunctionalized gold nanorods can be used as force transducers in single molecule experiments, where through the gold nanorods forces as high as tens of piconewtons can be transferred to the biological system. As the nanorods align in the trap, they could also be used as nanorotators, for example, by using a circularly polarized trapping laser instead of a linearly polarized laser.[30] By combination optical tweezers with polarized-dark field microscopy,[6] it would then even be possible to follow orientational changes of the particles in the trap and to use the aspect ratio for fine-tuning the applied torque.

Acknowledgment. We thank S. N. S. Reihani for help with the setup and him as well as P. M. Bendix for stimulating discussions. This work was funded by the Villum Kann Rasmussens Foundation through Bionet and the German Academy of Sciences Leopoldina through Grant BMBF-LPD 9901/8-164.

Supporting Information Available: Figures showing representative TEM images, distributions of length, width, and aspect ratio, and DDA calculations of the real part of the polarizability as a function of volume and divided by volume as a function of aspect ratios. This material is available free of charge via the Internet at http://pubs.acs.org.

References

(1) Lal, S.; Link, S.; Halas, N. J. *Nat. Photon.* **2007**, *1*, 641–648.
(2) Anker, J. N.; Hall, W. P.; Lyandres, O.; Shah, N. C.; Zhao, J.; Van Duyne, R. P. *Nat. Mater.* **2008**, *7*, 442–453.
(3) Sönnichsen, C.; Franzl, T.; Wilk, T.; von Plessen, G.; Feldmann, J.; Wilson, O.; Mulvaney, P. *Phys. Rev. Lett.* **2002**, *88*, 077402.
(4) Farrer, R. A.; Butterfield, F. L.; Chen, V. W.; Fourkas, J. T. *Nano Lett.* **2005**, *5*, 1139–1142.
(5) Pérez-Juste, J.; Pastoriza-Santos, I.; Liz-Marzán, L. M.; Mulvaney, P. *Coord. Chem. Rev.* **2005**, *249*, 1870–1901.
(6) Sönnichsen, C.; Alivisatos, A. P. *Nano Lett.* **2005**, *5*, 301–304.
(7) Yguerabide, J.; Yguerabide, E. E. *Anal. Biochem.* **1998**, *262*, 137–156.
(8) Wang, H.; Huff, T. B.; Zweifel, D. A.; He, W.; Low, P. S.; Wei, A.; Cheng, J.-X. *Proc. Natl. Acad. Sci.U.S.A.* **2005**, *102*, 15752–15756.
(9) Durr, N. J.; Larson, T.; Smith, D. K.; Korgel, B. A.; Sokolov, K.; Ben-Yakar, A. *Nano Lett.* **2007**, *7*, 941–945.
(10) Chithrani, B. D.; Ghazani, A. A.; Chan, W. C. W. *Nano Lett.* **2006**, *6*, 662–668.
(11) Pierrat, S.; Zins, I.; Breivogel, A.; Sonnichsen, C. *Nano Lett.* **2007**, *7*, 259–263.
(12) Grier, D. G. *Nature* **2003**, *424*, 810–816.
(13) Svoboda, K.; Block, S. M. *Opt. Lett.* **1994**, *19*, 930–932.
(14) Hansen, P. M.; Bhatia, V. K.; Harrit, N.; Oddershede, L. *Nano Lett.* **2005**, *5*, 1937–1942.
(15) Bosanac, L.; Aabo, T.; Bendix, P. M.; Oddershede, L. B. *Nano Lett.* **2008**, *8*, 1486–1491.
(16) Pelton, M.; Liu, M.; Kim, H. Y.; Smith, G.; Guyot-Sionnest, P.; Scherer, N. F. *Opt. Lett.* **2006**, *31*, 2075–2077.
(17) Toussaint, K. C.; Liu, M.; Pelton, M.; Pesic, J.; Guffey, M. J.; Guyot-Sionnest, P.; Scherer, N. F. *Opt. Express* **2007**, *15*, 12017–12029.
(18) Nikoobakht, B.; El-Sayed, M. A. *Chem. Mater.* **2003**, *15*, 1957–1962.
(19) Oddershede, L.; Grego, S.; Nørrelykke, S. F.; Berg-Sørensen, K. *Probe Microsc.* **2001**, *2*, 129–137.
(20) Reihani, S. N. S.; Oddershede, L. B. *Opt. Lett.* **2007**, *32*, 1998–2000.
(21) Dreyer, J. K.; Berg-Sørensen, K.; Oddershede, L. *Appl. Opt.* **2004**, *43*, 1991–1995.
(22) Kress, H.; Stelzer, E. H. K.; Rohrbach, A. *Appl. Phys. Lett.* **2004**, *84*, 4271–4273.
(23) Dienerowitz, M.; Mazilu, M.; Reece, P. J.; Krauss, T. F.; Dholakia, K. *Opt. Express* **2008**, *16*, 4991–4999.
(24) Agayan, R. R.; Gittes, F.; Kopelman, R.; Schmidt, C. F. *Appl. Opt.* **2002**, *41*, 2318–2327.
(25) Bohren, C.; Huffman, D. *Absorption and Scattering of Light by Small Particles*; John Wiley & Sons: New York, 1982.
(26) Berg-Sørensen, K.; Oddershede, L.; Florin, E.-L.; Flyvbjerg, H. *J. Appl. Phys.* **2003**, *93*, 3167–3176.
(27) Berg-Sørensen, K.; Flyvbjerg, H. *Rev. Sci. Instrum.* **2004**, *75*, 594–612.
(28) Hansen, P. M.; Tolic-Nørrelykke, I.; Flyvbjerg, H.; Berg-Sørensen, K. *Comput. Phys. Commun.* **2006**, *175*, 572–573.
(29) Singer, W.; Nieminen, T. A.; Gibson, U. J.; Heckenberg, N. R.; Rubinsztein-Dunlop, H. *Phys. Rev. E* **2006**, *73*, 021911.
(30) La Porta, A.; Wang, M. *Phys. Rev. Lett.* **2004**, *92*, 190801.
(31) Tirado, M. M.; López Martínez, C.; de la Torre, J. G *J. Chem. Phys.* **1984**, *81*, 2047–2052.
(32) Löwen, H. *Phys. Rev. E* **1994**, *50*, 1232–1242.
(33) Seol, Y.; Carpenter, A. E.; Perkins, T. T. *Opt. Lett.* **2006**, *31*, 2429–2431.
(34) Hoekstra, A. G.; Frijlink, M.; Waters, L. B. F. M.; Sloot, P. M. A. *J. Opt. Soc. Am. A* **2001**, *18*, 1944–1953.
(35) http://www.science.uva.nl/research/scs/Software/adda/index.html, available online.
(36) Johnson, P. B.; Christy, R. W. *Phys. Rev. B* **1972**, *6*, 4370.

NL802053H